Dalton Transactions

ROYAL SOCIETY OF CHEMISTRY

PAPER

View Article Online
View Journal | View Issue

Cite this: *Dalton Trans.*, 2025, **54**, 11056

Osmium–terpyridine complexes linked with stilbene-coupled naphthalene, anthracene, and pyrene moieties act as multichannel sensors for F^- and Hg^{2+} *via* non-classical interactions†

Tanusree Ganguly, Tuhin Abedin and Sujoy Baitalik *

Fluoride (F^-) and mercuric (Hg^{2+}) ion sensing behaviours of homoleptic Os(II)–terpyridine complexes coupled with stilbene-appended naphthalene, anthracene and pyrene motifs have been thoroughly investigated here through the intermediacy of multiple non-covalent interactions such as CH···F hydrogen bonding, anion–π and cation–π interactions. The interaction event is monitored by absorption, steady state and time-resolved emission, and ^1H, ^{19}F and ^{13}C NMR spectroscopy. The stilbene units in the complexes enable *trans–trans* (*t–t*) to *cis–cis* (*c–c*) photoisomerization upon exposure to light, accompanied by substantial reorientation of their molecular backbone. In order to examine the efficiency of the conformational change in the ion binding characteristics, both anion and cation sensing investigations are also conducted on the *c–c* form of the complexes. Substantial alteration in sensing efficacy is indeed observed on passing from the *t–t* to the *c–c* forms of the complexes, highlighting the role of conformation changes in the ion–receptor interactions. The ion sensing efficacy of the *trans–trans* (*t–t*) forms is found to be higher relative to their *cis–cis* (*c–c*) counterparts. Parallel to the experimental study, computational investigations were also conducted on the *t–t* and *c–c* conformers of the complexes to elucidate various non-covalent interactions that are operative during the interplay among the complexes with both F^- and Hg^{2+} ions.

Received 14th May 2025,
Accepted 17th June 2025

DOI: 10.1039/d5dt01134e

rsc.li/dalton

Introduction

Supramolecular interaction has garnered considerable attention in numerous areas at the forefront of chemistry and biology.[1–6] Non-covalent interactions, *viz.* van der Waals forces, hydrogen bonding, electrostatic, cation–π, CH–π, anion–π and π–π stacking interactions, to name a few, govern the assembly and functionality of such supramolecular architectures.[2–8] Although weak, these interactions play a fundamental role in preserving the essential structures of vital biological molecules like DNA, RNA, and proteins.[9–12] The significance of these weak interactions has also opened up new frontiers in the field of supramolecular chemistry of ions encompassing both anion and cation recognition, sensing, and transport.[13–20]

Designing of phosphorescent materials emitting in the near-infrared (NIR) and IR region is now gaining great attention for their potential applications in biology, chemistry, and technology.[21–25] NIR light, by virtue of its low interference and invisibility, could be safely used for sensing of specific anions and cations in biological systems.[21–31] Chemosensors, often constructed through covalent or non-covalent coupling of binding sites and signaling subunits, operate as meticulously designed molecular systems. When suitably designed, these systems are capable of transforming guest binding interactions into recognizable signals accompanied by considerable changes in the absorption, emission and redox behaviours.[21–31] Among the various output signals, those stemming from modifications in emission spectral characteristics are particularly compelling, and quite a large number of chromogenic and fluorogenic chemosensors have already been documented for sensing of selected anions and cations.[32–35]

In this work, our main objective is to utilize NIR-emissive receptors that are capable of multi-channel recognition of selected anions and cations through the intermediacy of various non-covalent interactions. In order to accomplish our objective, we employed herein a new class of our recently reported $Os[(tpy\text{-}pvp\text{-}X)_2](ClO_4)_2$ complexes consisting of a polyaromatic unit such as anthracene, naphthalene and pyrene at the 4′ position of the terpyridine moiety having an absorption and emission spectral window in the visible region

Department of Chemistry, Inorganic Chemistry Section, Jadavpur University, Kolkata 700032, India. E-mail: sbaitalik@hotmail.com, sujoy.baitalik@jadavpuruniversity.in; Tel: +91-033-2414-6666

† Electronic supplementary information (ESI) available. See DOI: https://doi.org/10.1039/d5dt01134e

and stretching into the NIR domain (Chart 1).[36] By virtue of the presence of extended π-conjugation *via* stilbene units together with polyaromatic hydrocarbons, the present complexes are expected to recognize specific anions and cations through the intermediacy of multiple non-covalent interactions, *viz*. hydrogen bonding, cation–π, CH–π, anion–π and π–π stacking interactions. We would like to mention that the complexes are highly soluble in polar aprotic solvents like MeCN and DMSO while being sparingly soluble in aqueous medium.

Upon complexation with the Os^{2+} ion, the terpyridine and other aromatic protons within the complex backbone are expected to become acidic to some extent, enabling them to participate in C–H···A^--type (A = anion) hydrogen bonding interactions with anions.[37–42] Anion recognition and sensing are paramount due to their pivotal roles in chemical and biological processes. Due to its relevance in environment and biology, we have focused herein on designing effective chemosensors for F^-. A diverse array of receptor motifs incorporating hydrogen bond donors, such as $NH_{urea/thiourea}$, $NH_{imidazole/pyrrole/indole}$, NH_{amide} and $OH_{phenol/catechol}$, have been extensively utilized as the primary binding motifs in the design of chemosensors, with their mechanisms and functions thoroughly explored in numerous reviews.[43–51] Now, by virtue of having a delocalized π-acidic electron cloud, the present complexes are expected to interact with selected anions through anion–π interactions.[52–54] Relative to the ubiquitous cation–π interactions, the anion–π interactions are less explored due to their ostensibly counterintuitive nature. Since these interactions are mostly dependent on the distance, anion–π interactions are comparatively weaker than the cation–π interactions because the van der Waals radii of anions are larger than those of cations.[55,56] Leveraging the favourable photophysical and electrochemical properties, coupled with the presence of multiple acidic C–H protons and electron-rich π-electron delocalized polyaromatic motifs, the anion-sensing characteristics of the complexes are comprehensively investigated in this work through multiple optical channels and spectroscopic techniques.

Among the heavy metals, mercury (Hg) poses significant health and environmental risks due to its toxic, persistent, and non-biodegradable nature.[57–59] Once released into the environment, mercury can accumulate into the ecosystems and contaminate soil, water, and food chains. This bioaccumulation of Hg can lead to severe health issues in humans, including neurological damage, kidney failure, Minamata disease, and developmental disorders, particularly when exposure occurs through contaminated water or seafood.[60,61] Due to these dangers, regulatory agencies such as the World Health Organization (WHO) and the Environmental Protection Agency (EPA) enforce strict limits on mercury levels to minimize its harmful effects on both human health and the environment.[62,63] Optical detection methods, such as fluorescence and colorimetric changes, are highly convenient due to their simplicity and sensitivity, with fluorescent probes offering the key advantage of intracellular detection.[64–69] The presence of polyaromatic moieties within their architecture makes the present complexes rich in π-electron density. Consequently, interaction with cationic moieties is likely to be energetically favourable. Additionally, cation–π interactions should also be operative, governed by electrostatic forces and cation-induced polarization.[70] Cation–π interactions are crucial in fields like chemistry, biology, and materials science, playing significant roles in processes such as steroid biosynthesis, acetylcholine receptor binding and ion selectivity in potassium channels.[71–74] Initially thought to be purely electrostatic, these interactions also involve induction, dispersion, and covalent contributions, particularly in transition metal cation–π systems.[71,75–78] While studies predominantly focus on main group cations like Li, Na, and K, transition metal based cation–π interactions, especially with M^{2+}···π systems, are less explored due to the complexity of their open-shell electronic structures.[79–84] Despite some research on transition metal–polyaromatic hydrocarbon complexes,[85–87] their untapped potential in the field of toxic metal sensing offers a promising avenue for advancing detection technologies. Due to the toxic nature of the Hg^{2+} ion, we have concentrated on developing chemosensors specifically tailored for its detection. Although there is documentation of cation–π and very few instances of anion–π interactions in metal complexes,[79–92] to the best of our knowledge, there are no reports of such interactions based on Os(II)–terpyridine type complexes. This is the first report wherein the present Os–terpyridine complexes display simultaneous anion–π and cation–π interactions with F^- and Hg^{2+}, respectively.

Incorporation of a stilbene unit makes room for the *t–c* photoisomerization upon shining light which in turn will reorient the conformation of the polyaromatic moieties within the complex backbone.[93–97] Thus, it is quite expected that the

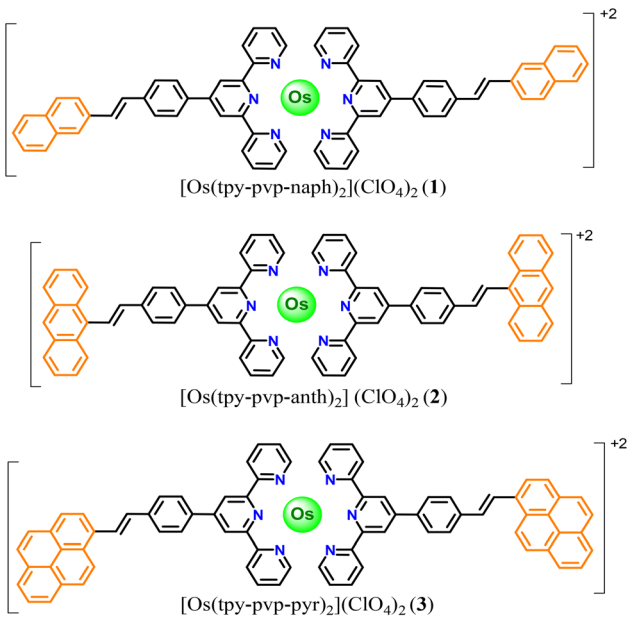

Chart 1 The ChemDraw structures of the Os(II) complexes.

extent of both anion–π and cation–π interactions will change among the two isomeric forms of the complexes. To this end, we will also thoroughly investigate the anion and cation sensing experiments with the *cis*-form of the complexes. In conjunction with experimental demonstration, computational analysis using density functional theory and time-dependent DFT has been executed to obtain the electronic properties of the molecular systems and the mode of ion–receptor interactions.

Experimental section

Materials

Reagent grade chemicals and solvents used in the present investigation are purchased from local vendors. Tpy-pvp-X (X = naphthalene, anthracene, and pyrene) ligands are prepared and characterized using our reported method.[95]

Synthesis of the metal complexes

The homoleptic Os(II)–terpyridine complexes are synthesized upon refluxing K_2OsCl_6 and the respective ligand (tpy-pvp-X) in a 1 : 2 ratio under an argon atmosphere in an ethylene glycol medium, followed by their ion exchange with sodium perchlorate ($NaClO_4$). Purification of the complexes is accomplished by column chromatography and recrystallization from appropriate solvent(s). The detailed synthesis and characterization of the complexes have been meticulously discussed in our recently reported literature.[36]

Instruments and physical methods

Details of instruments and physico-chemical measurements are provided in the ESI.†

Results and discussion

Overview of the photophysical, electrochemical and photoisomerization behaviours

The synthesis, characterization, and photophysical, electrochemical and photoisomerization behaviors of the Os(II) complexes were previously reported by our group.[36] A brief summary of the photophysical, electrochemical and reversible *trans–cis* photo-isomerization behaviours of the complexes is again narrated here for the sake of the readers. All three complexes display an intense band at ~500 nm, corresponding to singlet Os(d) → tpy(π*) charge transfer (^{1}MLCT) transitions, and a broad and weaker band beyond 500 nm due to $\{^1[Os^{II}(d\pi)^6] \rightarrow {}^3[Os^{II}(d\pi)^5tpy(\pi^*)^1]\}$ charge transfer (^{3}MLCT) transitions. The peaks within 400–314 nm indicate mixed MLCT and ILCT transitions, while the intense bands below 300 nm are attributed to π–π* transitions. Upon excitation in the ^{1}MLCT region, all complexes exhibit a single broad, structureless phosphorescent band in the NIR range (736–756 nm) at RT, dependent on the polyaromatic hydrocarbon moiety. The lifetimes of the complexes lie in the range of 84.5–112.5 ns. Electrochemical studies reveal a reversible Os^{2+}/Os^{3+} oxidation within the domain of 0.93–0.96 V and multiple reduction peaks for terpyridine units at −1.10 to −1.85 V.

The complex undergoes *t–t* to *c–c* isomerization due to the presence of an ethylenic double bond, upon irradiation with a 500 nm light source. A gradual decrease in the absorption of MLCT and ILCT band intensities occurs and the spectral lines are found to pass through clear isosbestic points. The emission intensity varies with the nature of the substituent, either increasing or decreasing, while the emission maximum remains unchanged. The time taken to saturate varies between 19 and 542 min, depending on the substituent. Reversible *c–c* to *t–t* isomerization is also feasible upon irradiation with 270 nm light, wherein the complex almost reverts back to its initial *t–t* state which is again monitored *via* absorption and emission spectroscopy. Finally, substantial modulation of the rate of photo-isomerization was also achieved *via* oxidation with ceric ammonium nitrate as well as reduction with metallic sodium.

Anion sensing behaviours of the complexes

The anion sensing characteristics of **1–3** are systematically investigated in MeCN *via* different optical channels and spectroscopic techniques. Tetrabutylammonium (TBA) salts of F^-, Cl^-, Br^-, I^-, CN^-, AcO^- and $H_2PO_4^-$ are utilized for this purpose. The absorption and emission spectral responses of the complexes in the presence of the studied anions are depicted in Fig. 1 and Fig. S1, S2 (ESI†). Amongst the anions, F^- induces the maximum change while the remaining anions are unable to induce any detectable change in their spectral profile.

To acquire quantitative insight about the receptor–anion interplay, we performed titration experiments upon gradual addition of F^- and monitored the changes *via* absorption and emission spectroscopy (Fig. 2). In the absorption spectra, a decrease in the absorbance of the MLCT and ILCT bands occurs with a concomitant increase in the π–π* band intensities for both **2** and **3**. For **1**, a simultaneous increase in the absorbance of both ILCT and π–π* bands takes place together with a small decrease in the absorbance of the MLCT bands. The decrease in the absorbance of the MLCT band is the maximum for **2**, while minimum for **1**. All the spectral lines pass through one or more isosbestic points indicating the presence of two or more species in equilibrium with one another. Complete saturation occurs upon addition of 92 equivalents of F^-. On the emission side, upon excitation at 450 nm, the emission intensity of the peak at ~740 nm slightly decreases with concomitant rise of a new peak at ~530 nm for all three complexes. The peak in the shorter wavelength region is generally due to the ligand-centred emission arising out of the deactivation of the ^{3}ILCT state, while the lower energy band at a longer wavelength (~740 nm) emerges due to deactivation from the ^{3}MLCT state.[94] Continued addition of F^- results in enormous intensification of the shorter wavelength peak and ultimately saturates at 92 equiv. An increase in the *Φ*

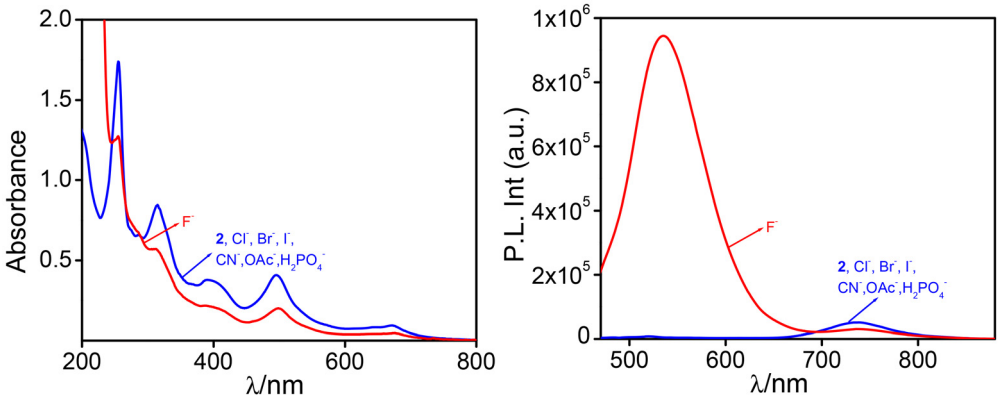

Fig. 1 Absorption (left) and emission (right, λ_{ex} = 450 nm) spectra of **2** in MeCN (1.0 × 10^{-5} M) in the absence and presence of studied anions as their TBA (tetrabutylammonium) salts.

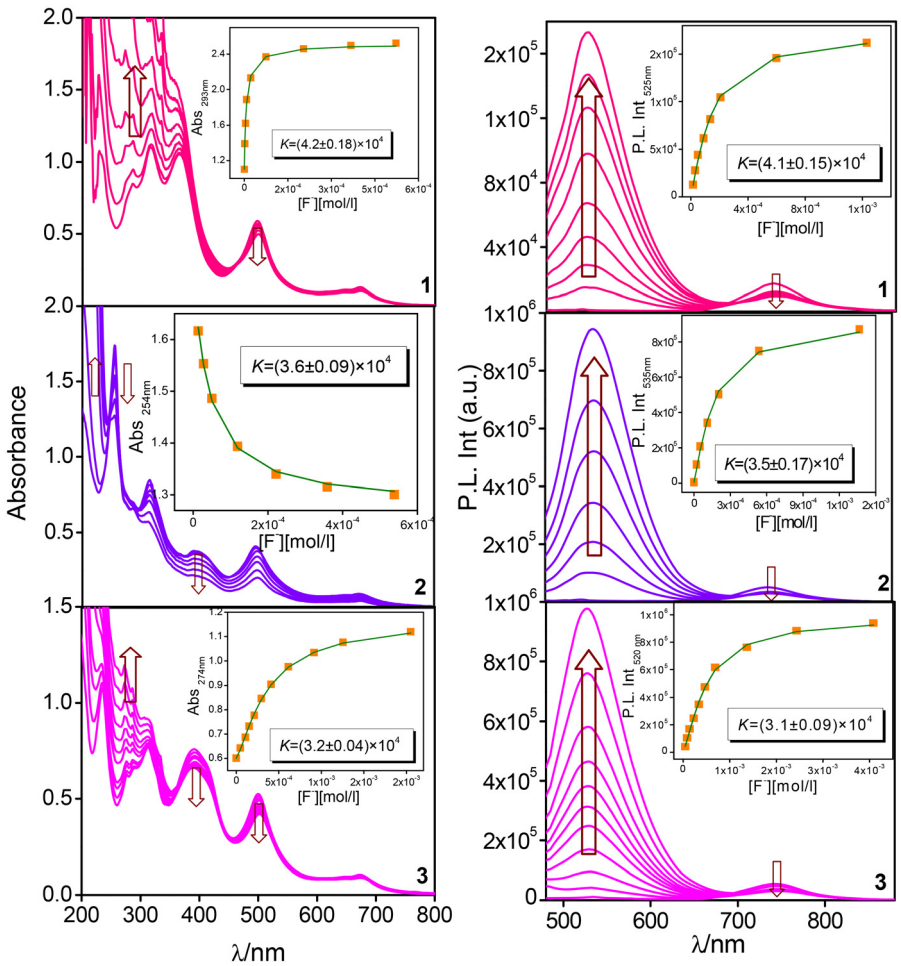

Fig. 2 Absorption (left panel) and emission (λ_{ex} = 450 nm) (right panel) titration profiles of the *t*–*t* forms of **1–3** in MeCN upon gradual addition of F^-. Insets of the figures in both left and right panels indicate the estimation of binding constants.

value is also noticed for the F^- saturated solutions. We have also measured the lifetime values of the complexes upon F^- addition and the corresponding decays are illustrated in Fig. S3 (ESI†). The lifetime values are seen to decrease in the case of **1** and **2**, while it increases for **3**, albeit to a very small extent.

We have also carried out the titration experiments in predominantly water medium as well as on a solid surface. Due to

solubility limitation of the present complexes in pure water, we prepared a 1 : 10 MeCN–H_2O (v/v) solution of two complexes {**1** (naphthalene) and **2** (anthracene)} and executed their anion sensing behaviours (Fig. S4, ESI†). A gradual decrease in absorbance along with a small red-shift of the ^{1}MLCT band is observed in both cases. On the emission side, a decrease in intensity of the ^{3}MLCT band occurs together with a systematic increase in intensity of the ^{1}ILCT band. Similarity in terms of trend in the spectral profiles is observed in both the media, although the extent of change in MeCN–H_2O is comparatively less than that in pure MeCN. The lesser change in both the absorbance and emission spectral profile is probably due to the trapping of F^- by the water molecules. We have also measured the lifetime values of the complexes upon F^- addition and the corresponding decays are illustrated in Fig. S5 (ESI†). The lifetime value increases for **1**, while it decreases for **2**. We also dropcast all three complexes on the quartz surface and recorded their emission spectra in both their free and anion bound states and presented them in Fig. S6 (ESI†). Substantial enhancement in the emission intensity of the ^{3}MLCT band takes place in all three complexes in the presence of only F^- among the studied anions. For the anthracene derivative, intensification of the ^{3}ILCT also occurs. The emission behavior of the complexes in the solution state, on the other hand, is found to be opposite relative to their solid state with the exception of the anthracene derivative, wherein intensities of both ^{3}ILCT and ^{3}MLCT increase, albeit to different extents.

To elucidate the probable mode of interaction, a ^{1}H NMR titration experiment is executed upon systematic addition of F^- to the DMSO-d_6 solution of **1** and the corresponding profile is displayed in Fig. 3. It is observed that the signals due to $H_{3'}$, H_6 and H_7 undergo significant downfield shift and the extent of shift varies between 0.1 and 0.3 ppm. The well-resolved doublets for the H_6 proton, initially observed at 9.13 ppm, split into two new doublets at 9.21 and 9.09 ppm. As F^- is gradually added, one of the doublets shift towards the up-field region while the other one towards the downfield region as shown in Fig. 3. Change in multiplicity is also observed for H_8, H_4, H_{11}, H_{14} and H_{16} protons, which undergo an up-field shift, resulting in the formation of a multiplet. The ethylenic protons, H_9 and H_{10}, also exhibit a slight up-field shift. The H_3 proton experiences a small up-field shift, while the H_5 proton undergoes a small downfield shift. Upon complexation with Os^{2+}, the terpyridine and other aromatic protons within the complexes acquired acidic properties, facilitating their involvement in hydrogen bonding interactions with incoming F^- guests. The observed chemical shifts in selected proton signals in the presence of F^- ions could be due to the occurrence of a combination of non-covalent interactions, including CH···F hydrogen bonding, CH–π, and anion–π interactions. It is to be noted that the integration count of the total number of protons in the F^- saturated spectrum increases relative to its initial form which is indicative of some sort of association among the complex molecules.

To investigate the mode of receptor–anion interaction, we also conducted ^{19}F NMR titration experiments by gradually adding the anthracene (**2**) derivative to a DMSO-d_6 solution of TBAF. The corresponding spectral profiles are shown in Fig. S7 (ESI†). Free TBAF exhibits a strong singlet at −106.9 ppm, corresponding to the F^- ion. Upon addition of the complex, the singlet peak undergoes a slight upfield shift and gradually

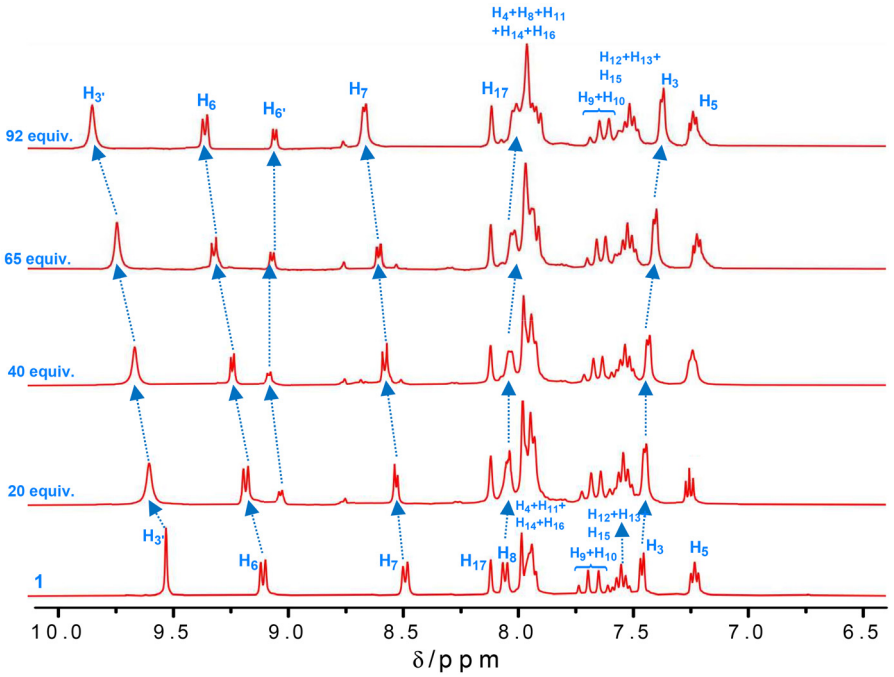

Fig. 3 ^{1}H NMR spectral titration of the *t*–*t* form of **1** upon incremental addition of TBAF (tetrabutylammonium fluoride) in DMSO-d_6.

diminishes, indicating the formation of the complex···F^- adduct. Notably, no additional peaks appear during the titration, confirming the absence of covalent attachment of fluorine to the complex backbone. Thus, the ^{19}F NMR spectral analysis strongly supports the occurrence of non-classical interactions between the complexes and F^- ions.

We further determined the binding constants (K) for the receptor–anion interactions by analyzing the absorption and emission titration data of the t–t form of the complexes, using eqn (S1) (ESI†) for 1 : 2 stoichiometry (inset of Fig. 2 and Fig. S4, ESI†). The resulting K values are summarized in Table 1 and found to vary within a small range of 1.2–4.2 × 10^4. Additionally, the detection limits of the complexes for F^- are calculated that range between 1.0×10^{-6} and 8.5×10^{-8} M {Table 1 and Fig. S8, S9 (ESI†)}.

An increase in the integration count of the total number of protons in the ^1H NMR spectrum of complex **1** prompted us to conduct the dynamic light scattering (DLS) experiments {Fig. S10 (ESI†)}. The DLS spectra are acquired in MeCN for the free as well as F^- saturated forms of the complexes. It is seen that the size of the particle increases from 3–84 nm to 23–460 nm on addition of F^-. Taking into consideration that no additional solvent is used in the DLS experiment, the possibility of solvent-induced aggregation is eliminated. Therefore, the aggregation primarily occurs due to non-covalent interactions drawing the molecules closer together, effectively increasing their size. As aggregation is known to enhance emission through the restriction of intramolecular motions (RIM), the observed increase in emission intensity upon F^- addition can be attributed to this phenomenon. Despite an increase in the total integration count of the protons, no evidence for the formation of a dimer-type adduct is observed. Consequently, the results of both NMR and DLS experiments clearly suggest the formation of aggregates mediated by F^- ions.

Since the conformation of the molecules significantly alters on moving from the t–t to the c–c form, it is expected that the extent of different non-classical interactions would also be substantially modified. To this end, we investigated the anion sensing characteristics of the c–c form of the complexes and compared them with their t–t counterparts. The absorption and emission spectral change in the c–c form of the complexes is monitored upon stepwise inclusion of F^- (Fig. 4). A closer inspection reveals that there is a marked difference in the spectral pattern of the c–c form relative to the t–t isomer of the respective complex. In the absorption spectra, F^- addition leads to an increase in absorbance of the MLCT and ILCT bands along with a small decrease in the π–π* band intensity. Interestingly, the spectral window stretches up to ~1000 nm in the case of **1** and **3** in the presence of F^-. Again, all the spectral lines pass through clear isosbestic points, indicating that two or more species are in equilibrium with each other. Spectral saturation takes place upon addition of ~86 equiv. of F^- for the c–c form of the complexes. In the emission spectra, the c–c forms of the complexes display two bands at ~500 and 740 nm. The former peak is attributed to the ligand centred (ILCT) emission, while the peak at 740 nm corresponds to the MLCT emission. Upon F^- addition, the MLCT peak intensity gradually decreases while that of the ligand-centered band increases. We have also measured the lifetimes of the F^--saturated c–c forms of complexes, wherein a small decrease in lifetime is noticed for all cases, albeit to different extents {Fig. S11 (ESI†)}.

To elucidate the probable mode of interaction, a ^1H NMR titration experiment is also executed on the c–c form of **2** upon systematic addition of F^- in DMSO-d_6 and the corresponding profile is displayed in Fig. 5. We have already provided the ^1H NMR spectra of the anthracene derivative (**2**) due to photoisomerization in our previously reported manuscript.[36] It is observed that two sets of proton peaks exist: the residual proton signals of the complex moiety due to their t–t form and the proton peaks arising out of their isomerised c–c forms. Fluoride addition affects both types of protons in the NMR spectrum. The protons associated with $H_{3'}$ at 9.60 ppm and $H_{3''}$ at 9.47 ppm experience a downfield shift to 9.90 and 9.67 ppm, respectively. The multiplet corresponding to H_6 and $H_{6'}$, having their chemical shift position within 9.17–9.08 ppm, also shifts downfield, resulting in two doublets at 9.44 and

Table 1 Equilibrium constants (K) and detection limits for **1–3** towards F^- and Hg^{2+} in MeCN and 1 : 10 MeCN–H_2O (v/v)

	Binding constant				Detection limit/M			
	F^-		Hg^{2+}		F^-		Hg^{2+}	
Compounds	Absorption	Emission	Absorption	Emission	Absorption	Emission	Absorption	Emission
MeCN								
1(t–t)	4.2×10^4	4.1×10^4	4.8×10^4	4.7×10^4	1.3×10^{-7}	8.5×10^{-8}	1.7×10^{-7}	3.2×10^{-8}
2(t–t)	3.6×10^4	3.5×10^4	2.7×10^4	3.4×10^4	1.6×10^{-7}	2.0×10^{-7}	7.9×10^{-7}	6.5×10^{-7}
3(t–t)	3.2×10^4	3.1×10^4	3.6×10^4	3.9×10^4	7.8×10^{-7}	4.9×10^{-7}	4.0×10^{-7}	2.9×10^{-7}
1(c–c)	3.4×10^4	3.6×10^4	2.9×10^4	2.7×10^4	4.1×10^{-7}	2.4×10^{-7}	5.6×10^{-7}	3.9×10^{-7}
2(c–c)	2.9×10^4	2.7×10^4	3.4×10^4	3.3×10^4	7.1×10^{-7}	6.0×10^{-7}	3.1×10^{-7}	1.6×10^{-7}
3(c–c)	2.4×10^4	2.2×10^4	2.1×10^4	2.4×10^4	9.5×10^{-7}	9.2×10^{-7}	1.2×10^{-6}	1.0×10^{-6}
1 : 10 MeCN–H_2O (v/v)								
1(t–t)	7.9×10^3	1.2×10^4	5.8×10^3	3.6×10^3	1.0×10^{-6}	2.5×10^{-6}	1.0×10^{-5}	1.0×10^{-6}
2(t–t)	7.2×10^3	9.1×10^3	4.9×10^3	4.2×10^3	3.3×10^{-6}	1.9×10^{-6}	9.3×10^{-6}	2.4×10^{-6}

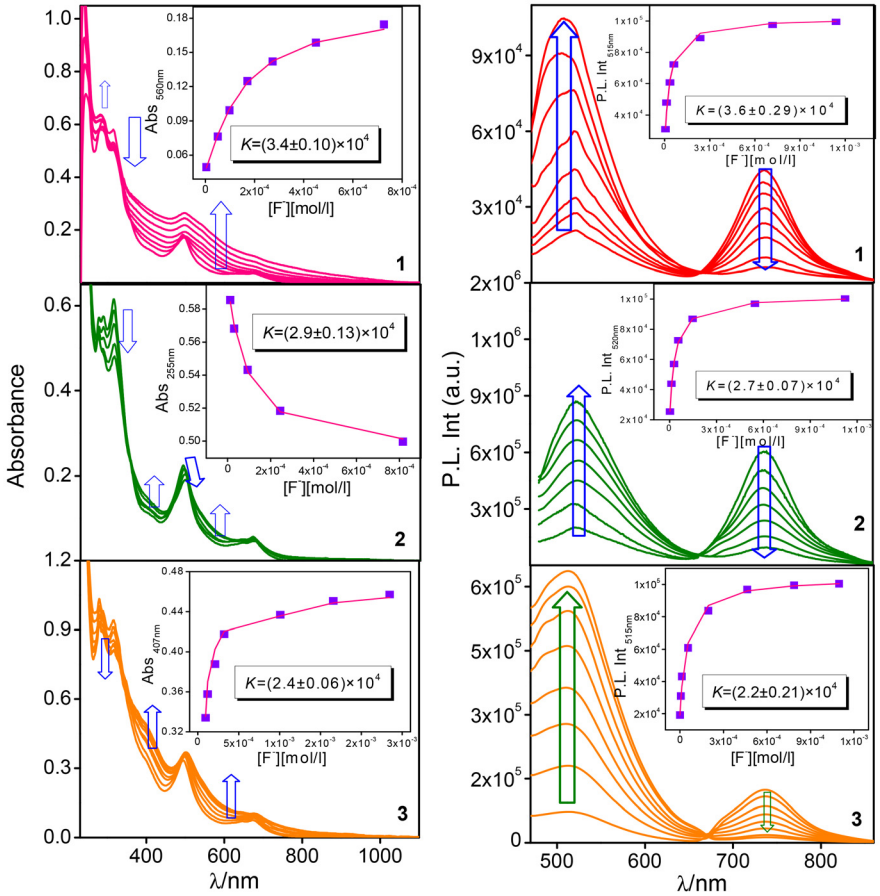

Fig. 4 Absorption (left panel) and emission (λ_{ex} = 450 nm) (right panel) titration profiles of the *c*–*c* forms of **1**–**3** in MeCN upon gradual addition of F^-. Insets of the figures in both left and right panels indicate the estimation of binding constants.

9.31 ppm. The $H_{7'}$ proton at 8.56 ppm experiences a slight downfield shift, forming a multiplet within the 8.88–8.76 ppm range. A significant downfield shift from 8.13 to 8.51 ppm also takes place for the $H_{15'}$ proton (singlet linked with the *c*–*c* form of the anthracene moiety). Interestingly, apart from the $H_{15'}$, most of the protons associated with the anthracene moiety undergo an up-field shift accompanied by changes in their multiplicities. Upon addition of up to 25 equiv. of F^-, the $H_{9'}$ and $H_{10'}$ protons associated with the ethylenic bond exhibit a slight up-field shift from their initial positions of 6.87 and 6.65 ppm to 6.75 and 6.48 ppm, respectively. However, upon the addition of 84 equiv. of F^-, they undergo a pronounced downfield shift to 7.16 and 6.75 ppm, respectively. The observed down-field shift of the abovementioned protons is probably due to C–H···F hydrogen bonding interactions. The peaks due to terpyridine protons (H_3–H_6) undergo both up-field and downfield shifts together with a change in their multiplicities, indicating the occurrence of some sort of interactions among the complex moiety and the incoming F^-. The observed shifts in selected proton signals in the presence of F^- can be attributed to the interplay of various non-classical interactions, including CH···F hydrogen bonding, as well as CH–π and anion–π interactions. A significant increase in strain is induced across the complex backbone on moving from their *t*–*t* to *c*–*c* forms. Consequently, the extent of C–H···F^- interaction between the different protons with incoming F^- will alter on passing from *t*–*t* to *c*–*c* analogues.

We also determined the binding constants (K) for the receptor–anion interactions in the *c*–*c* form of the complexes by analyzing their absorption and emission titration data and upon employing eqn (S1) (ESI†) for 1 : 2 stoichiometry (presented in the inset of Fig. 4). It is observed that the values of K for the *c*–*c* forms are lower compared to those for their analogous *t*–*t* isomers and the observed values for the *c*–*c* forms lie in the order **1** > **2** > **3**. The enhanced sensitivity of the *t*–*t* forms of the complexes over their *c*–*c* isomers towards F^- is also reflected in the extent of change in their absorption and emission spectral profiles. This lowering of the binding value most probably arises due to the increased strain generated in the *c*–*c* form of the complexes. The limits of detection towards F^- in the *c*–*c* forms of the complexes are also calculated and found to range between 2.4×10^{-7} and 9.5×10^{-6} M, which are lower than those of their analogous *t*–*t* isomers {Table 1 and Fig. S12 (ESI†)}.

To obtain direct proof for the occurrence of non-covalent interactions, we conducted DFT calculations on the *t*–*t* as well

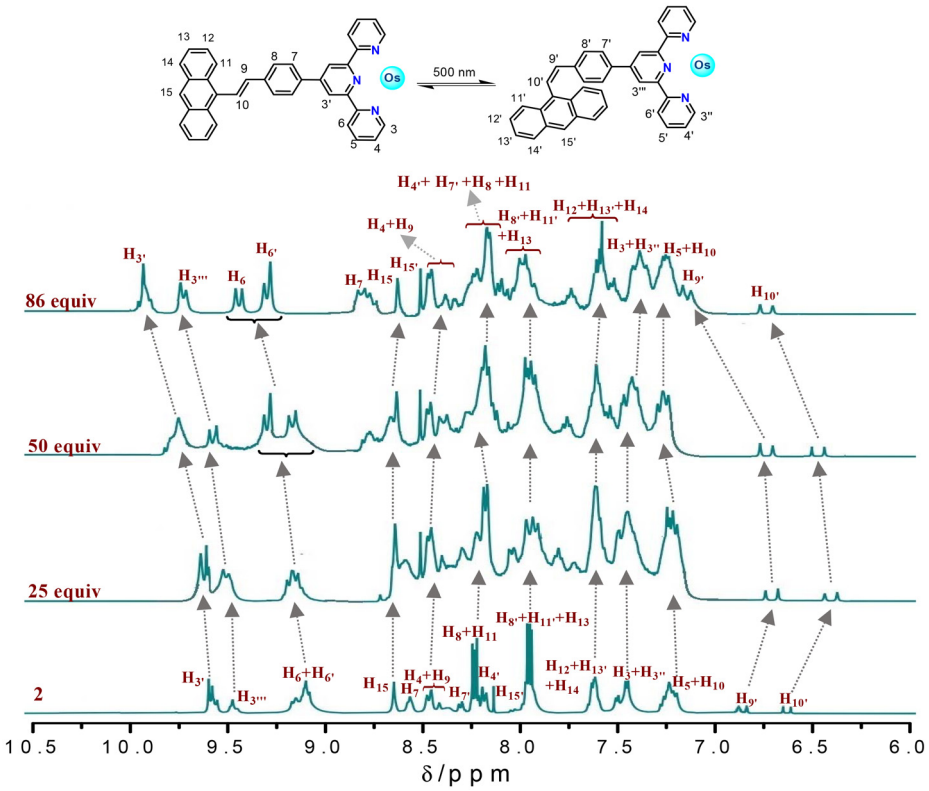

Fig. 5 ^{1}H NMR spectral titration of the *c*–*c* form of **2** upon incremental addition of TBAF (tetrabutylammonium fluoride) in DMSO-d_6.

as *c*–*c* forms of the complexes and calculated the energy values associated with each mode of interaction (Fig. 6). We first optimized the ground state geometry of **1** in both of its *t*–*t* and *c*–*c* states and calculated their energy values (A and D, respectively). Next, we computed the energy due to interaction with F^- at some specified positions of the complex. We mainly considered two types of non-covalent interactions, *viz*. CH···F^- hydrogen bonding and anion–π interactions. Initially, geome-

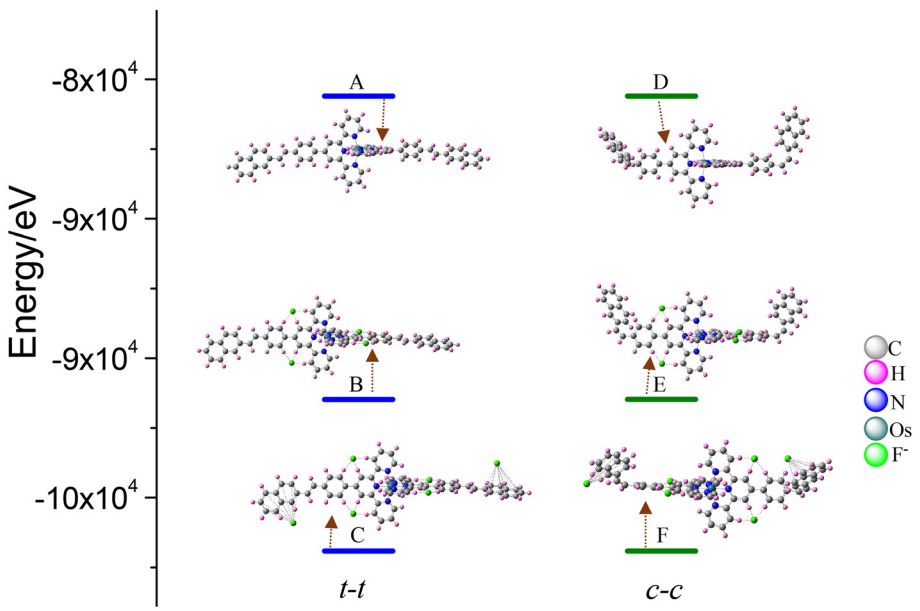

Fig. 6 Calculated energy diagram showing decrease in the energy of the **1**···F^- complex adduct due to CH···F^- and anion–π interactions in the *t*–*t* and *c*–*c* forms of **1**.

tries involving only CH···F^- interactions within the terpyridine and styrylbenzene moieties are optimized. Four feasible CH···F^- interactions (B and E) are identified, and their energy values are found to decrease relative to their free forms. This is followed by optimization of geometries including both F^-–π and CH···F interactions within the single entity (C and F). The energy is lower than the rest of the optimized structures, indicating that the increase in non-covalent interactions stabilizes the complex···F^- adduct. Although the energy of the complex decreases upon F^- addition, there is no much energy difference between the different isomerized states of the complex.

Cation sensing behaviours of the complexes

Since the complexes possess a delocalized π-electron cloud throughout the entire complex backbone, we are also interested in investigating the cation sensing characteristics of the complexes. The cation sensing behaviours of **1–3** are systematically investigated in MeCN *via* different optical channels and spectroscopic techniques. We tested for a wide variety of cations, *viz*. Li^+, Na^+, K^+, Be^{2+}, Mg^{2+}, Ca^{2+}, Zn^{2+}, Cd^{2+} and Hg^{2+}, wherein a significant change in their absorption and emission spectra is exhibited by Hg^{2+} only {Fig. 7 and Fig. S13, S14 (ESI†)}.

Fig. 8 shows the change in the absorption and emission spectra of the acetonitrile solution of the complexes upon addition of $HgCl_2$. In the absorption spectra, a gradual decrease in absorbance of the MLCT band is unanimously observed in all three complexes while a small increase in absorbance of the mixed ILCT and π–π* band takes place in the case of **1** and **3** only. All the spectral lines pass through one or more isosbestic points, indicating that two species are in equilibrium with each other. Interestingly, a broad band arises in the NIR region of ~700–1100 nm for **1**. Regarding their emission properties, **1** and **3** demonstrate a gradual decrease in emission intensity, while **2** exhibits an increase in emission intensity. Notably, the emission maximum (λ_{max}) remains unchanged for all three complexes. The lifetimes of the Hg^{2+}-saturated solutions of the complexes are also measured. It is observed that Hg^{2+} induces a significant decrease in lifetime values of **1** and **3**, while a minor increase is noticed for **2**, with respect to their *t*–*t* analogues {Fig. S15 (ESI†)}. The observed change in spectral properties could be due to non-classical interaction between the π-electron cloud of the complex backbone and the Hg^{2+} ion.

We also executed the cation sensing behaviours of two complexes {**1** (naphthalene) and **2** (anthracene)} in 1 : 10 MeCN–H_2O (v/v) in the presence of Hg^{2+}. A gradual decrease in absorbance along with a small red-shift (~6 nm) of the ^{1}MLCT band is observed in both cases {Fig. S16 (ESI†)}. In the case of emission, the intensity also decreases systematically upon gradual addition of Hg^{2+} to the complex solutions. The extent of change in their spectral profiles is found to be relatively less compared to that in MeCN. We have also measured the lifetime of the complexes wherein the value decreases for both **1** and **2** {Fig. S17 (ESI†)}. Again, we dropcast all the three complexes on the quartz surface and recorded their emission spectra in both their free and cation-bound states {Fig. S18 (ESI†)}. Substantial quenching of ^{3}MLCT emission takes place in all three complexes in the presence of only Hg^{2+} among the studied cations.

To obtain direct proof for the cation–π interactions, we also recorded the ^{13}C NMR spectrum of the *t*–*t* form of **1** in DMSO-d_6 upon addition of 95 equiv. of Hg^{2+} {Fig. S19 (ESI†)}. It is noticed that most of the ^{13}C NMR peaks of the Hg^{2+}-saturated solution are shifted towards the downfield region by ~0.20–2.71 ppm. This observation is probably due to the dragging of electron density from the $C^{\delta-}$ units in the complex framework by the Hg^{2+} ions. This change in the ^{13}C NMR peak position clearly indicates the occurrence of some sort of non-covalent interactions between the complex cation and Hg^{2+}, thereby leading to the formation of a **1**···Hg^{2+} adduct.

We also carried out the DLS study of the complexes in their Hg^{2+}-saturated forms to speculate any change in the particle size upon addition of the cation {Fig. S20 (ESI†)}. Surprisingly, the particle size increases from 3–84 nm to 102–146 nm, indicating the occurrence of some sort of association upon addition of Hg^{2+} ions. As previously discussed, since no other solvent is involved, the observed increase in particle size is

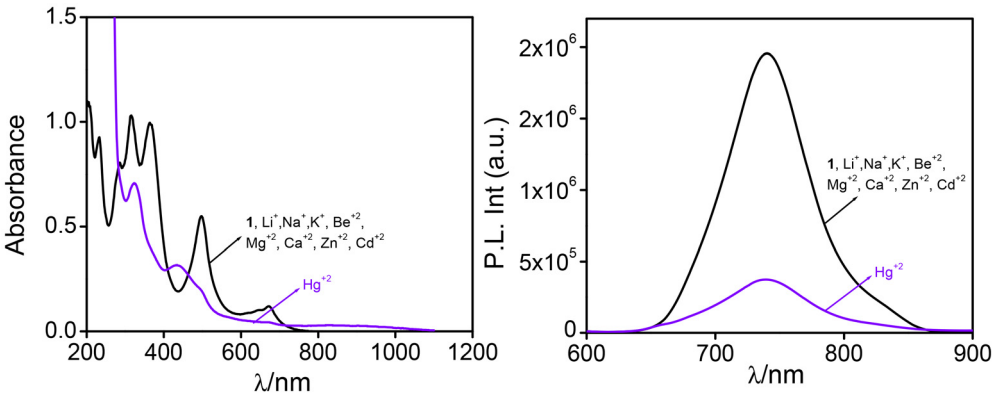

Fig. 7 Absorption (left) and emission (right, λ_{ex} = 500 nm) spectra of **1** in MeCN (1.0 × 10^{-5} M) in the absence and in the presence of studied cations.

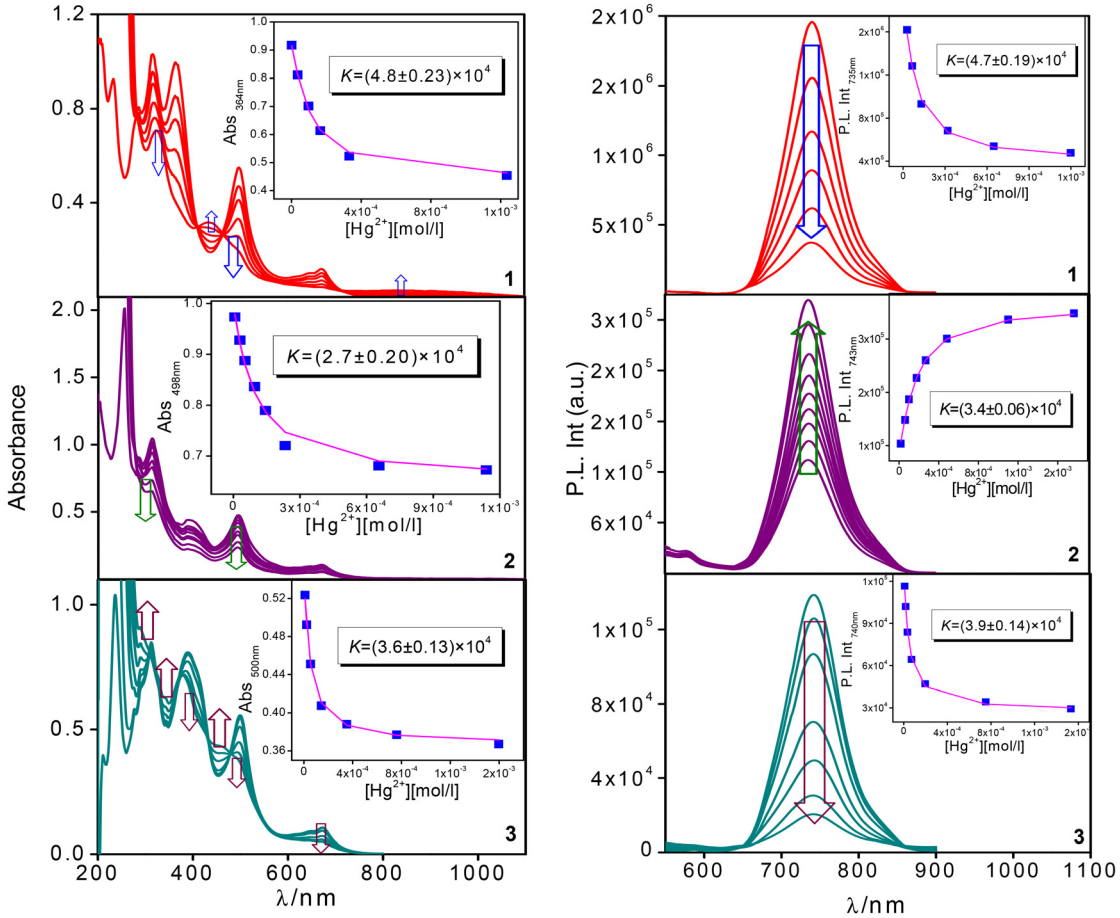

Fig. 8 Absorption (left) and emission (right, λ_{ex} = 500 nm) spectral changes upon incremental addition of Hg^{2+} to the *t*–*t* form of **1**–**3** (1.0 × 10^{-5} M) in MeCN solution. Insets of the figures in both left and right panels indicate the estimation of binding constants.

solely due to the addition of Hg^{2+}, which in turn induces some sort of association. This aggregation arises from non-covalent interactions that bring the molecules closer, increasing their size.

Since the structural orientations of the complexes are significantly altered on moving from the *t*–*t* to the *c*–*c* form, we are also interested in investigating the efficacy of the *c*–*c* form of the complexes to interact with the Hg^{2+} ions. The changes are again monitored by absorption and emission spectroscopy (Fig. 9). It is of interest to see that the nature of the change in the absorption spectra is substantially altered, wherein the MLCT and ILCT bands lose their intensity together with a small increase in the absorbance of the π–π* bands. All the spectral lines again pass through an isosbestic point, indicating that two or more species are in equilibrium with one another. In the emission spectra, when excited at 450 nm, **1** and **2** exhibit a decrease in the emission intensity of the MLCT band, while the ligand-centered band remains unaffected. In contrast, for **3**, an increase in the intensity of the MLCT band takes place with a concomitant decrease in that of the ligand-centred band. The lifetime of the complexes is found to decrease upon addition of Hg^{2+} to their *c*–*c* forms {Fig. S21 (ESI†)}.

To quantitatively evaluate the receptor–cation interactions, binding constants (*K*) are determined by analyzing the absorption and emission titration data of the complexes {inset of Fig. 9 and Fig. S16 (ESI†)}, utilizing the 1 : 2 binding model as described by eqn (S1) (ESI†). While for the *t*–*t* forms, the binding constants lie in the range of 3.6 × 10^3–4.8 × 10^4, for the respective *c*–*c* forms, they lie in the range of 2.1–3.4 × 10^4 (Table 1). The data clearly indicate that the *K* values for receptor–mercury (Hg^{2+}) interactions in their *c*–*c* forms are consistently lower relative to their corresponding *t*–*t* isomers. This decrease in binding affinity can be attributed to the structural changes induced during *c*–*c* isomerization, which likely alter the spatial arrangement and electronic environment of the binding site, reducing its ability to interact strongly with ions. The order of the binding constants is **1** > **3** > **2** for the *t*–*t* form, while for the *c*–*c* form, the order is **2** > **1** > **3**. This reflects the influence of polyaromatic hydrocarbon substituents on the receptor's binding efficacy, suggesting that both steric and electronic effects play a critical role in modulating the receptor's cation recognition capabilities. The detection limits of the complexes towards Hg^{2+} are also found to be substantially higher in the *t*–*t* form (1.0 × 10^{-5} to 7.9 × 10^{-7} M) compared

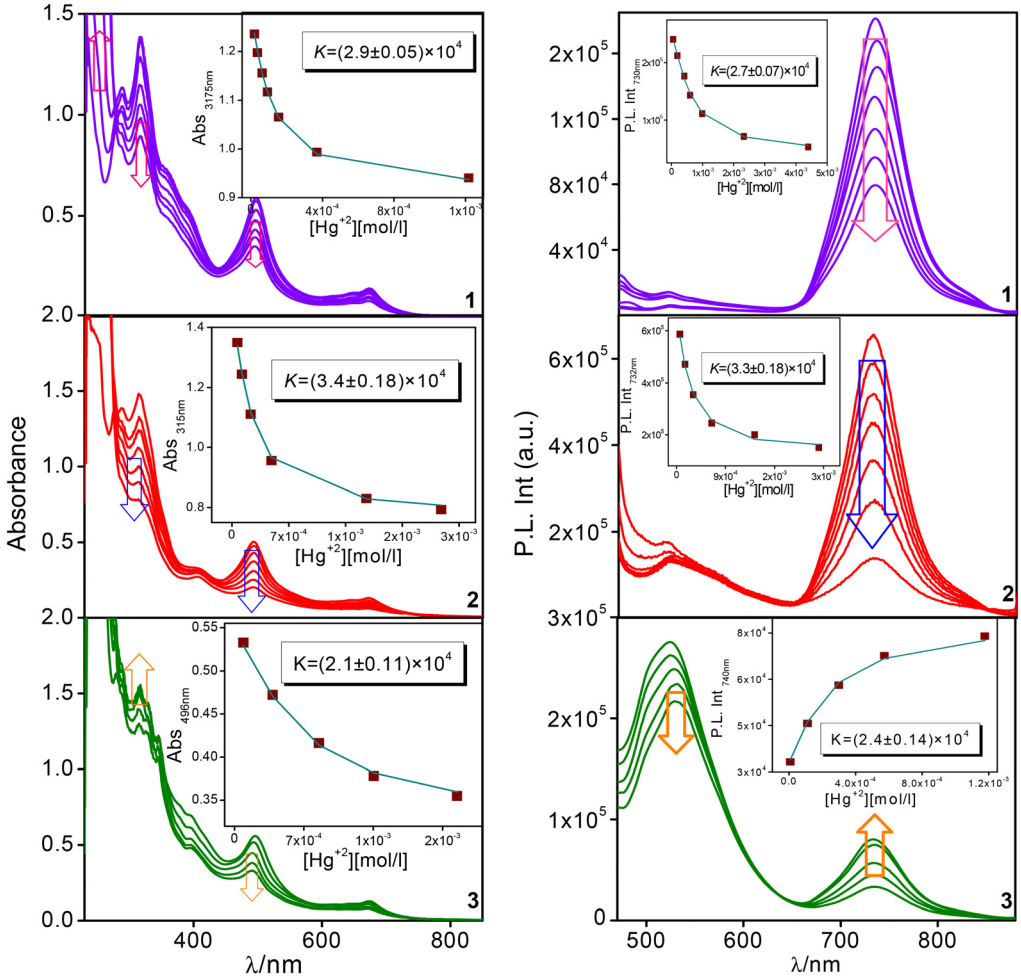

Fig. 9 Absorption (left) and emission (right, λ_{ex} = 450 nm) spectral changes upon incremental addition of Hg^{2+} to the *c*–*c* form of **1**–**3** (1.0×10^{-5} M) in MeCN solution. Insets of the figures in both left and right panels indicate the estimation of binding constants.

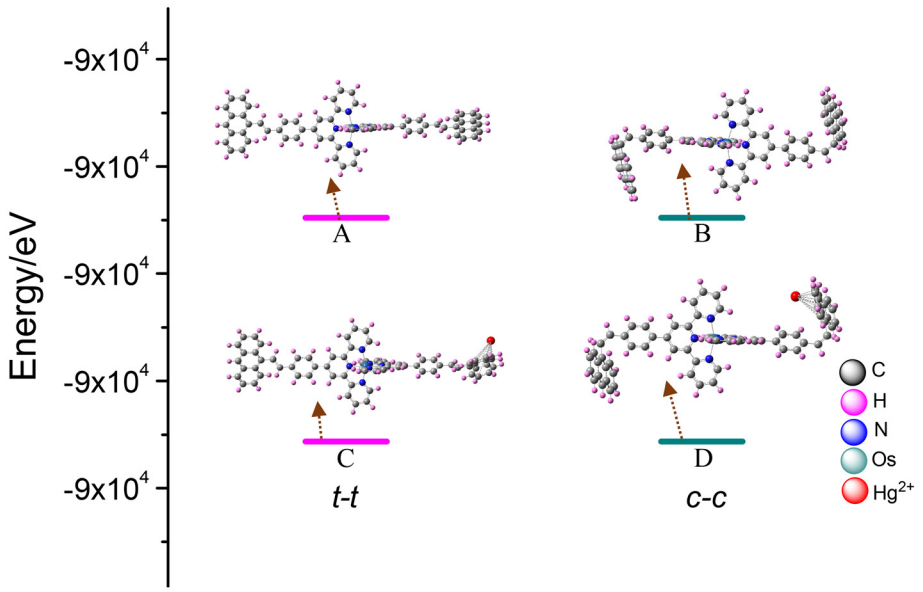

Fig. 10 Calculated energy diagram showing decrease in the energy of the **2**···Hg^{2+} complex adduct due to Hg^{2+}···π interactions in the *t*–*t* and *c*–*c* forms of **2**.

with their *c–c* isomers (1.6×10^{-7} to 1.2×10^{-6} M) {Table 1 and Fig. S22–24 (ESI†)}.

To obtain direct evidence for the occurrence of non-covalent interactions, we also conducted DFT calculations on the *t–t* as well as the *c–c* form of the complexes and estimated the corresponding interaction energy values (Fig. 10). The electrostatic potential (ESP) plots of complex **2** are generated for both *t–t* and *c–c* states to identify electron density distribution across the complex backbone (Fig. S25, ESI†). The electron-dense region is indicated by green colour while the electron-deficient regions are designated by blue colour. Subsequently, the ground-state geometries of complex **2** in both conformations are optimized, and their respective energy values (A and B) are calculated. Following this, we evaluated the interaction energy associated with the π-electron cloud of the complex and Hg^{2+} at the identified electron-dense regions (C and D). The results indicate that the Hg^{2+}–π-interaction decreases the overall energy of the adduct, ultimately stabilizing at a significantly lower energy compared to its initial state, although not much variation is observed upon moving from the *t–t* to the *c–c* form.

Conclusions

With regard to our sustained interest in designing prospective molecular sensors and switches that function in the near-infrared (NIR) domain, we employed herein a new array of homoleptic Os(II)–terpyridine complexes coupled with stilbene-appended naphthalene, anthracene and pyrene motifs for the simultaneous recognition of a selective anion and cation. The complexes are found to selectively sense F^- among a wide range of anions and Hg^{2+} amongst the cations *via* multiple optical channels and spectroscopic techniques. The results of absorption and steady-state and time-resolved emission experiments together with ^1H, ^{13}C, and ^{19}F NMR spectroscopic analyses and dynamic light scattering (DLS) experiments unequivocally demonstrate strong association among the complexes and F^- as well as Hg^{2+} ions. These interactions arise from a sophisticated interplay of non-classical forces, including CH···F hydrogen bonding, CH–π, anion–π, and cation–π interactions, and through-space electrostatic attraction between the complex and the F^- and Hg^{2+} ions.

The stilbene units in the complexes enable *t–t* → *c–c* photoisomerization upon exposure to light, which subsequently reorients the conformation of the stilbene-coupled polyaromatic moieties within the complex framework. In order to examine the efficiency of conformational changes in the ion binding characteristics, both anion and cation sensing investigations are also conducted on the *c–c* form of the complexes. Substantial alteration in sensing efficacy is indeed observed on passing from the *t–t* to the *c–c* form of the complexes, highlighting the role of conformation changes in the ion–receptor interactions. In conjunction with experimental demonstration, computational analysis using density functional theory has been executed to elucidate the mode of ion–receptor interplay. In essence, the present Os(II)–terpyridine complexes act as potential multichannel sensors working in the NIR domain.

Author contributions

T. Ganguly and T. Abedin carried out the chemical investigations. T. Ganguly performed data organization. S. Baitalik supervised and validated this project. The manuscript was written by T. Ganguly and S. Baitalik.

Conflicts of interest

The authors declare no competing financial interest.

Data availability

The data supporting this article have been included in the ESI.†

Details of instruments and methods, additional experimental data, figures and tables related to ^1H, ^{19}F, and ^{13}C NMR, absorption and emission spectral measurements, and DLS and DFT calculations are provided in the attached ESI.†

Acknowledgements

S. B. acknowledges the SERB [grant no. CRG/2020/001233] and the CSIR [grant no. 01(2945)/18/EMR-II], New Delhi. T. A. acknowledges the UGC-JRF fellowship. TCSPC facilities under the DST-FIST (I and II) and DST-PURSE program of the Department of Chemistry (JU) are also gratefully acknowledged.

References

1 A. J. Neel, M. J. Hilton, M. S. Sigman and F. D. Toste, *Nature*, 2017, **543**, 637.
2 D. X. Wang and M.-X. Wang, *Acc. Chem. Res.*, 2020, **53**, 1364–1380.
3 H. T. Chifotides and K. R. Dunbar, *Acc. Chem. Res.*, 2013, **46**, 894–906.
4 F. Biedermann and H.-J. Schneider, *Chem. Rev.*, 2016, **116**, 5216.
5 A. Haque, K. M. Alenezi, M. S. Khan, W. Y. Wong and P. R. Raithby, *Chem. Soc. Rev.*, 2023, **52**, 454–472.
6 D.-X. Wang and M.-X. Wang, *Acc. Chem. Res.*, 2020, **53**, 1364–1380.
7 L. M. Salonen, M. Ellermann and F. Diederich, *Angew. Chem., Int. Ed.*, 2011, **50**, 4808–4842.
8 A. Y. Y. Tam, K. M. C. Wong, G. Wang and V. W.-W. Yam, *Chem. Commun.*, 2007, 2028–2030.
9 S. Burley and G. Petsko, *Science*, 1985, **229**, 23–28.

10 S. Li, V. R. Cooper, T. Thonhauser, B. I. Lundqvist and D. C. Langreth, *J. Phys. Chem. B*, 2009, **113**, 11166–11172.
11 X. Xiu, N. L. Puskar, J. A. P. Shanata, H. A. Lester and D. A. Dougherty, *Nature*, 2009, **458**, 534.
12 T. Steiner and G. Koellner, *J. Mol. Biol.*, 2001, **305**, 535–557.
13 V. Gorteau, G. Bollot, J. Mareda, A. Perez-Velasco and S. Matile, *J. Am. Chem. Soc.*, 2006, **128**, 14788–14789.
14 D.-H. Tuo, W. Liu, X.-Y. Wang, X.-D. Wang, Y.-F. Ao, Q.-Q. Wang, Z.-Y. Li and D.-X. Wang, *J. Am. Chem. Soc.*, 2019, **141**, 1118–1125.
15 Y. Zhao, Y. Cotelle, L. Liu, J. Lopez-Andarias, A.-B. Bornhof, M. Akamatsu, N. Sakai and S. Matile, *Acc. Chem. Res.*, 2018, **51**, 2255–2263.
16 G.-G. Ramírez, E. C. Escudero-Adan, J. Benet-Buchholz and P. Ballester, *Angew. Chem., Int. Ed.*, 2008, **47**, 4114–4118.
17 H. Zhao, L. Tang, Y. Fang, C. Liu, W. Ding, S. Zang, Y. Chen, W. Xu, Y. Yuan, D. Fang, *et al.*, *J. Am. Chem. Soc.*, 2023, **145**, 16406–16416.
18 N. Zacharias and D. A. Dougherty, *Trends Pharmacol. Sci.*, 2002, **23**, 281–287.
19 S. Tsuzuki, *Interactions with aromatic rings*, Springer, Berlin, 2005, vol. 115.
20 X. Zhang, X. Hao, L. Liu, A.-T. Pham, J. Lopez-Andarias, A. Frontera, N. Sakai and S. Matile, *J. Am. Chem. Soc.*, 2018, **140**, 17867–17871.
21 X. Michalet, F. F. Pinaud, L. A. Bentolila, J. M. Tsay, S. Doose, J. J. Li, G. Sundaresan, A. M. Wu, S. S. Gambhir and S. Weiss, *Science*, 2005, **307**, 538–544.
22 C.-J. Yao, Y.-W. Zhong, H.-J. Nie, H. D. Abruña and J. Yao, *J. Am. Chem. Soc.*, 2011, **133**, 20720–20723.
23 M. Bar, D. Maity, S. Deb, S. Das and S. Baitalik, *Dalton Trans.*, 2017, **46**, 12950–12963.
24 A. Paul, T. Ganguly, M. Bar and S. Baitalik, *Inorg. Chem.*, 2021, **60**, 412–422.
25 V. Bulach, F. Sguerra and M. W. Hosseini, *Coord. Chem. Rev.*, 2012, **256**, 1468–1478.
26 H. Wang, J.-Y. Shao, R. Duan, K.-Z. Wang and Y.-W. Zhong, *Dalton Trans.*, 2021, **50**, 4219–4230.
27 J.-Y. Shao, W.-W. Yang, J. Yao and Y.-W. Zhong, *Inorg. Chem.*, 2012, **51**, 4343–4351.
28 N. Busschaert, C. Caltagirone, W. V. Rossom and P. A. Gale, *Chem. Rev.*, 2015, **115**, 8038–8155.
29 S. Mardanya, S. Karmakar, D. Mondal and S. Baitalik, *Inorg. Chem.*, 2016, **55**, 3475–3489.
30 D. Mondal, S. Biswas, A. Paul and S. Baitalik, *Inorg. Chem.*, 2017, **56**, 7624–7641.
31 D. Maity, C. Bhaumik, D. Mondal and S. Baitalik, *Dalton Trans.*, 2014, **43**, 1829–1845.
32 R. M. Máñez and F. Sancenón, *Chem. Rev.*, 2003, **103**, 4419–4476.
33 C. I. David and H. I. Lee, *Microchem. J.*, 2024, 110359.
34 M. Ilakiyalakshmi, K. Dhanasekaran and A. A. Napoleon, *Top. Curr. Chem.*, 2024, **382**, 29.
35 S. Dutta and A. Sahana, *Anal. Methods*, 2024, **16**, 344–370.
36 T. Ganguly, T. Abedin, D. Maity and S. Baitalik, *Inorg. Chem.*, 2025, **64**, 4415–4430.
37 L. Flamigni, F. Barigelletti, N. Armaroli, B. Ventura, J.-P. Collin, J.-P. Sauvage and J. A. G. Williams, *Inorg. Chem.*, 1999, **38**, 661–667.
38 S. Develay, O. Blackburn, A. L. Thompson and J. A. G. Williams, *Inorg. Chem.*, 2008, **47**, 11129–11142.
39 Y. M. Dikova, D. S. Yufit and J. A. G. Williams, *Inorg. Chem.*, 2023, **62**, 1306–1322.
40 D. Maity, C. Bhaumik, D. Mondal and S. Baitalik, *Inorg. Chem.*, 2013, **52**, 13941–13955.
41 D. Maity, C. Bhaumik, D. Mondal and S. Baitalik, *Dalton Trans.*, 2014, **43**, 1829–1845.
42 M. Bar, P. Pal, D. Maity and S. Baitalik, *Sens. Actuators, B*, 2018, **266**, 493–505.
43 Y. Zhou, J. F. Zhang and J. Yoon, *Chem. Rev.*, 2014, **114**, 5511–5571.
44 D. A. Jose, P. Kar, D. Koley, B. Ganguly, W. Thiel, H. N. Ghosh and A. Das, *Inorg. Chem.*, 2007, **46**, 5576–5584.
45 P. Das, P. Mahato, A. Ghosh, A. K. Mandal, T. Banerjee, S. Saha and A. Das, *J. Chem. Sci.*, 2011, **123**, 175–186.
46 A. Ghosh, S. Verma, B. Ganguly, H. N. Ghosh and A. Das, *Eur. J. Inorg. Chem.*, 2009, 2496–2507.
47 H. Singh, K. Tiwari, R. Tiwari, S. K. Pramanik and A. Das, *Chem. Rev.*, 2019, **119**, 11718–11760.
48 S. Guha and S. Saha, *J. Am. Chem. Soc.*, 2010, **132**, 17674–17677.
49 M. Cametti and K. Rissanen, *Chem. Soc. Rev.*, 2013, **42**, 2016–2038.
50 N. Kumari, N. Dey and S. Bhattacharya, *Analyst*, 2014, **139**, 2370–2378.
51 A. Balamurugan and H. Lee, *Sens. Actuators, B*, 2015, **216**, 80–85.
52 X. Zhang, X. Hao, L. Liu, A.-T. Pham, J. Lopez-Andarias, A. Frontera, N. Sakai and S. Matile, Primary, *J. Am. Chem. Soc.*, 2018, **140**, 17867–17871.
53 M. Mascal, A. Armstrong and M. D. Bartberger, *J. Am. Chem. Soc.*, 2002, **124**, 6274–6276.
54 I. Alkorta, I. Rozas and J. Elguero, *J. Am. Chem. Soc.*, 2002, **124**, 8593–8598.
55 M. S. Marshall, R. P. Steele, K. S. Thanthiriwatte and C. D. Sherrill, *J. Phys. Chem. A*, 2009, **113**, 13628–13632.
56 D. Quinonero, C. Garau, A. Frontera, P. Ballester, A. Costa and P. Deya, *J. Phys. Chem. A*, 2005, **109**, 4632–4637.
57 H. N. Kim, W. X. Ren, J. S. Kim and J. Yoon, *Chem. Soc. Rev.*, 2012, **41**, 3210–3244.
58 N. Chen, Y. Zhang, H. Liu, X. Wu, Y. Li, L. Miao, Z. Shen and A. Wu, *Sensors*, 2016, **1**, 521–527.
59 G. V. Ramesh and T. P. Radhakrishnan, *ACS Appl. Mater. Interfaces*, 2011, **3**, 988–994.
60 C. M. Carvalho, E. H. Chew, S. I. Hashemy, J. Lu and A. Holmgren, *J. Biol. Chem.*, 2008, **283**, 11913.
61 T. W. Clarkson, L. Magos and G. J. Myers, *N. Engl. J. Med.*, 2003, **349**, 1731–1737.
62 U.S. EPA. Draft Guidance for Implementing the January 2001, *Methylmercury Water Quality Criterion* [S]; EPA-823-R-01-001; Office of Science and Technology: Washington, DC, 2006, 1–20.

63 WHO. *Guideline Levels for Methylmercury in Fish* [S], CAC/GL7-1991; WHO: Geneva, Switzerland, 1991, 1.
64 A. Sigaeva, Y. Ong, V. G. Damle, A. Morita, K. J. van der Laan and R. Schirhagl, *Acc. Chem. Res.*, 2019, **52**, 1739–1749.
65 P. Broz, *Cell Res.*, 2016, **26**, 859–860.
66 J. Liu, J. C. Fraire, S. C. De Smedt, R. Xiong and K. Braeckmans, *Small*, 2020, **16**, 2000146.
67 S. P. Verma, C. Ghosh, A. J. Talreja, S. Pramanik, R. Sadhukhan, A. Mandal, A. Das, S. K. Samanta and D. K. Goswami, *ACS Appl. Electron. Mater.*, 2025, **7**, 1243–1251.
68 Y. Yang, H. Qi, X. Hou, M. Gao and S. Gong, *Crit. Rev. Anal. Chem.*, 2025, 1–17.
69 H. Lee, H. S. Lee, J. H. Reibenspies and R. D. Hancock, *Inorg. Chem.*, 2012, **51**, 10904–10915.
70 D. A. Dougherty, *Acc. Chem. Res.*, 2013, **46**, 885–893.
71 D. A. Dougherty, *Science*, 1996, **271**, 163–168.
72 E. S. Meadows, S. L. D. De Wall, L. J. Barbour and G. W. Gokel, *J. Am. Chem. Soc.*, 2001, **123**, 3092–3107.
73 A. S. Mahadevi and G. N. Sastry, *Chem. Rev.*, 2013, **113**, 2100–2138.
74 H. Minoux and C. Chipot, *J. Am. Chem. Soc.*, 1999, **121**, 10366–10372.
75 A. S. Reddy and G. N. Sastry, *J. Phys. Chem. A*, 2005, **109**, 8893–8903.
76 G. W. Gokel, L. J. Barbour, S. L. D. De Wall and E. S. Meadows, *Coord. Chem. Rev.*, 2001, **222**, 127–154.
77 I. Soteras, M. Orozco and F. J. Luque, *Phys. Chem. Chem. Phys.*, 2008, **10**, 2616–2624.
78 S. Tsuzuki, M. Mikami and S. Yamada, *J. Am. Chem. Soc.*, 2007, **129**, 8656–8662.
79 S. Kolakkandy, S. Pratihar, A. J. A. Aquino, H. Wang and W. L. Hase, *J. Phys. Chem. A*, 2014, **118**, 9500–9511.
80 F. Meyer and F. A. Khan, *J. Am. Chem. Soc.*, 1995, **117**, 9740–9748.
81 M. A. Duncan, *Int. J. Mass Spectrom.*, 2008, **272**, 99–118.
82 K. M. Wedderburn, S. Bililign, M. Levy and R. Gdanitz, *Chem. Phys.*, 2006, **326**, 600–604.
83 J. A. Maner, D. T. Mauney and M. A. Duncan, *J. Phys. Chem. Lett.*, 2015, **6**, 4493–4498.
84 P. B. Armentrout, B. Yang and M. T. Rodgers, *J. Phys. Chem. B*, 2013, **117**, 3771–3781.
85 T. D. Jaeger, D. van Heijnsbergen, S. J. Klippenstein, G. von Helden, G. Meijer and M. A. Duncan, *J. Am. Chem. Soc.*, 2004, **126**, 10981–10991.
86 A. C. Scott, J. W. Buchanan, N. D. Flynn and M. A. Duncan, *Int. J. Mass Spectrom.*, 2007, **266**, 149–155.
87 J. W. Buchanan, J. E. Reddic, G. A. Grieves and M. A. Duncan, *J. Phys. Chem. A*, 1998, **102**, 6390–6394.
88 W. Song, J. Gao, Y. Gao, G. G. Shan, Y. Geng, K. Shaoa and Z.-M. Su, *Inorg. Chem. Front.*, 2024, **11**, 1198.
89 S. Demeshko, S. Dechert and F. Meyer, *J. Am. Chem. Soc.*, 2004, **126**, 4508–4509.
90 B. L. Schottel, H. T. Chifotides, M. Shatruk, A. Chouai, L. M. Pérez, J. Bacsa and K. R. Dunbar, *J. Am. Chem. Soc.*, 2006, **128**, 5895–5912.
91 M. Capo, J. B. Buchholz and P. Ballester, *Inorg. Chem.*, 2008, **47**, 10190–10192.
92 E. Kuzniak, D. Pinkowicz, J. Hooper, M. Srebro-Hooper, L. Hetmańczyk and R. Podgajny, *Chem. – Eur. J.*, 2018, **24**, 16302–16314.
93 T. Ganguly, P. Pal, D. Maity and S. Baitalik, *J. Photochem. Photobiol., A*, 2023, **440**, 114662.
94 P. Pal, S. Mukherjee, D. Maity and S. Baitalik, *Inorg. Chem.*, 2018, **57**, 5743–5753.
95 T. Ganguly, P. Pal, A. Paul and S. Baitalik, *J. Photochem. Photobiol., A*, 2022, **430**, 113966.
96 V. W. W. Yam, V. C. Y. Lau and K. K. Cheung, Synthesis, Photophysics and Photochemistry of Novel Luminescent Rhenium(I) Photoswitchable Materials, *J. Chem. Soc., Chem. Commun.*, 1995, 259–261.
97 C. C. Ko and V. W. W. Yam, *J. Mater. Chem.*, 2010, **20**, 2063–2070.